Natural Hazards
and Earth System
Sciences
Discussions
Open Access
EGU

1   Hydrological control of large hurricane-induced lahars: evidences from rainfall,

2   seismic and video monitoring

3   Lucia Capra[1], Velio Coviello[1], Lorenzo Borselli[2], Víctor-Hugo Márquez-Ramírez[1], Raul

4   Arámbula-Mendoza[3]

5   *[1] Centro de Geociencias, Universidad Nacional Autónoma de México (UNAM), Campus*

6   *Juriquilla, Queretaro, México*

7   *[2] Instituto de Geología, Universidad Autónoma de San Luis Potosí, San Luis Potosí,*

8   *México*

9   *[3] Centro Universitario de Estudios e Investigaciones en Vulcanología (CUEIV),*

10   *Universidad de Colima, Colima, México.*

11

12   **Abstract**

13   The Volcán de Colima, one of the most active volcanoes in Mexico, is commonly affected

14   by tropical rains related to hurricanes that form over the Pacific Ocean. In 2001, 2013 and

15   2016 hurricanes Jova, Manuel and Patricia, respectively, ~~promoted~~ tropical storms that

16   accumulated up to 400 mm of rain in 36 hrs, with maximum intensities of 50 mm/hr~~s~~.

17   Effects were devastating, with the formation of multiple lahars along La Lumbre and

18   Montegrande ravines, which are the most active channels in sediment delivery on the S-SW

19   flank of the volcano. Deep erosion along the river channels and several landslides at their

20   side were observed, and damages to bridges and paved roads for the arrival of block-rich

21   fronts resulted in the distal reach of the ravines. Based on data from real-time monitoring

22   (including images, seismic records and rainfall data), the temporal sequence of these events

23   is reconstructed and analyzed with respect to the rainfall characteristics and the

24   hydrological response of the watersheds based on rainfall/infiltration numerical simulation.

Natural Hazards
and Earth System
Sciences
Discussions

25   For the studied events, lahars occurred after 5-6 hours since rainfall started, lasted several

26   hours and were characterized by several pulses with block-rich fronts and a maximum flow

27   discharge of 900 m^3/s. Rainfall/infiltration simulations were performer with the Flo-2D

28   code using the SCS-Curve number infiltration model. Results show different behaviors for

29   the arrival times of the first lahar pulses that correlate with the catchment's peak discharge

30   for La Lumbre ravine and with the peaks in rainfall intensity for Montegrande ravine. This

31   different behavior is strictly related to the area and shape of these two watersheds.

32   Nerveless, for all the analyzed cases, the largest lahar pulse always corresponds with the

33   last one and correlates with the maximum peak discharge of these catchments. Data here

34   presented show that main pulses within a lahar are not randomly distributed in time, and

35   they can be correlated with rainfall peak intensity and/or watershed discharge, depending

36   on the watershed area and shape. This outcome has important implications for hazard

37   assessment during extreme hydro-meteorological events since it could help in real-time

38   alert. A stormwater was here designed based on the rainfall time distribution of hurricanes

39   Manuel and Patricia and, in case on available weather forecasts, it can be used to run

40   simulations prior to the event, and have an estimation of the time arrivals of main pulses,

41   usually characterized by block-rich fronts that are responsible of damage to infrastructures

42   and loss of goods and lives.

43

44   ***Keywords****: lahar, hurricane, rainfall/infiltration simulation, Volcán de Colima, Mexico.*

45

46   **1. Introduction**

47   In past recent years hurricanes have had catastrophic effects on volcanoes of the

48   world triggering lahars (sediment-water gravity-driven flows on volcanoes). One of the

49   most recent episode is represented by the 2009 Hurricane Ida in El Salvador that caused

50   several landslides and debris flows from the Chichontepec volcano, killing 124 people, or

51   by the 1998 Hurricane Mitch that triggered the collapse of a small portion of the inactive

52   Casita volcano, originating a landslide that suddenly transformed into a lahar that

53   devastated several towns and killed 2000 people (Van Wyk Vries et al., 2000; Scott et al.,

54   2005). A similar event was observed in 2005 when tropical storm Stan triggered landslides

55   and debris flows from the Toliman Volcano (Guatemala), causing more than 400 fatalities

56   at Panabaj community (Sheridan et al., 2007). Other examples can be found at the

57   volcanoes Pinatubo (Philippines), Merapi and Semeru (Indonesia), Soufriére (Montserrat),

58   Mt. Ruapehu (New Zealand), where tropical storms and heavy rainfall seasons have

59   triggered high-frequency lahar events (Umbal and Rodolfo, 1996; Cronin et al., 1997;

60   Lavigne et al., 2000; Lavigne and Thouret, 2002; Barclay et al., 2007; Dumaisnil et al.,

61   2010; Doyle et al., 2010, de Bélizal et al., 2013).

62   Volcán de Colima (19°31'N, 103°37' W, 3860 m a.s.l., Fig. 1), one of the most

63   active volcanoes in Mexico, is periodically exposed to intense seasonal rainfalls that are

64   responsible for the occurrence of lahars from June to late October (Davila et al., 2007;

65   Capra et al., 2010). Rain-triggered lahars represent a very common process during the rainy

66   season (June-October) at Volcán de Colima (Davila et al., 2007; Capra et al., 2010;

67   Vazquez et al., 2016a). They usually affect areas as much as 15 km from the summit of the

68   volcano, with resulting damage to bridges and electric power towers (Capra et al., 2010),

69   and are more frequent just after eruptive episodes such as dome collapse emplacing block-

Natural Hazards
and Earth System
Sciences
Discussions

Open Access

EGU

70   and-ash flow deposits (Davila et al., 2007; Vázquez et al., 2016b). Several hurricanes

71   commonly hit the Pacific Coast each year and proceed inland as tropical rainstorm reaching

72   the Volcán de Colima area. In particular, on 2011, 2013 and 2015 Jova, Manuel and

73   Patricia hurricane respectively triggered long-lasting lahars along main ravines, causing

74   several damages on roads and bridges, leaven uncommunicated for few days several

75   communities in a radius of 15 km from the volcano.

76   Previous work (Davila et al., 2007; Capra et al., 2010) analyzed the lahars frequency

77   at Volcán de Colima in relation with the eruptive activity and the characteristics of

78   rainfalls. Lahars are more frequent at the beginning of the rains season, during short (< 1

79   hour) stationary rainfalls, with variable rainfall intensities and with only 10 mm of

80   accumulated rainfall. This behavior has been attributed to a hydrophobic effect of soils on

81   the volcano slope (Capra et al., 2010). In contrast, in the late rain season, when tropical

82   rainstorms are common, lahars are triggered depending on the 3-day antecedent rainfall and

83   with intensities that increase as the total rainfall amount increases (Capra et al., 2010). The

84   lahars record used for these previous studies was only based on seismic data. Since 2011 a

85   visual monitoring system have been installed on Montegrande and La Lumbre ravines

86   (Figure 1), based on which a quantitative characterization of some events (i.e type of flow,

87   velocity, flow discharge, flow fluctuation) have been possible (i.e. Vázquez et al., 2016a;

88   Coviello et al., under revision). The aim of the present paper is to better understand the

89   lahars initiation processes and their dynamical behavior, especially during hurricane events,

90   when more damages have been observed on inhabited area. In particular, the arrival time of

91   main lahar's front/surge at the monitoring stations is here analyzed with respect to the

92   rainfall characteristics (rain accumulation and intensity) in relation with the hydrological

93   response of the watersheds based on rainfall/infiltration numerical simulation. The

94   occurrence of discrete surges within lahars have been attributed to spatially and temporally

95   distributed lahar sources, temporary damming, progressive entrainment of bed material or

96   change in slope angle (i.e. Iverson 1997; Marchi et al. 2002; Takahashi 2007; Zanuttigh and

97   Lamberti 2007; Doyle et al., 2010; Kean et al., 2013). Without excluding previous models,

98   data here presented shows that main pulses within a lahar are not randomly distributed in

99   time, and they can be correlated with rainfall peak intensity and/or watershed discharge,

100   depending on the watershed shape and hydrophobic behavior subject to the antecedent soil

101   moisture. The lahars triggered by the hurricanes Jova, Manuel and Patricia are here used as

102   they correspond with the best documented events occurred during past years, and they will

103   be also compared with an extraordinary hydrometeorological event occurred at the begin of

104   the rain season (11 June, 2013) to better show the drastic change on lahar initiation due to

105   the hydrophobic effect of soils at Volcán de Colima. Based on rainfall distribution over

106   time for the analyzed events, a stormwater is here designed, whic can be used to run

107   simulations prior to an event to have an estimation of the time arrivals of main pulses when

108   weather forecast is available. The data here presented have important implication for hazard

109   assessment during extreme hydrometeorological events as a complementary tool of an early

110   warning system.

111

112   2. **Methods and data**

113   **2.1. La Lumbre and Montegrande watersheds**

Natural Hazards
and Earth System
Sciences
Discussions

114   The source area of lahars at Volcán de Colima corresponds to the uppermost unvegetated

115   portion of the cone (Fig. 1 and 2a), with slopes between 35° and 20°, that also corresponds

116   with an area of high connectivity, being prone to rills formation and erosive processes

117   (Ortiz et al., 2017). The channels along main ravines have slopes from 15° up to 4° in the

118   more distal reach, they are flanked by densely vegetated terraces, up to 15 m high in

119   average, that consist of debris avalanche and pyroclastic deposits from past eruptions (Figs.

120   2b and c) (Cortes et al., 2010; Roverato et al., 2011). Seven major watersheds from 2 to 14

121   km^2 feed the main ravines draining from the volcano on the southern side (Fig. 1). La

122   Lumbre is the largest watershed, with a total area of 14 km^2, and Montegrande is in average

123   with the other catchments, with an area of 2 km^2 (Fig. 1). Beside the difference in total

124   area, the Montegrande and La Lumbre watersheds are quite different in geometry.

125   Montegrande catchment is elongated, with a maximum width of 800 m, 300 m in average.

126   In contrast, the proximal portion of the La Lumbre catchment includes all the NW slope of

127   the cone, to then extent to a more elongated shape towards SW, being up to 1500 m in

128   width. These differences in area and shape can be correlated with a different response in

129   water discharge under a rainfall event. In circular drainages, as the proximal portion of the

130   La Lumbre watershed, all points are quite equidistant from the main river so all the

131   precipitation reaches the river at the same time, concentrating a large volume of water. In

132   contrast, in a more elongate basin, lateral drainages quickly drain water on the main

133   channel at different points but with a lower total discharge. The Gravelius's index Kg

134   (Bendjoudi and Hubert 2002), which is defined as the relation between the perimeter of the

135   watershed (P) and that of a circle having a surface equal to that of a watershed (A):

$$Kg = \frac{P}{2\sqrt{\pi A}}$$

Natural Hazards
and Earth System
Sciences
Discussions
Open Access
EGU

136   is here estimated for Montegrande watershed and for the upper, circular portion of La

137   Lumbre watershed obtaining values of 1.7 and 1.1 respectively. The lower the value, the

138   more regular the basin's perimeter and the more prone it is to present high runoff peaks.

139   Based on these considerations, at La Lumbre watershed a larger volume of water

140   concentrates along the main channel because of its larger surface and circular shape, but

141   after a larger period of time respect to Montegrande ravine, where a minor volume of water

142   quickly reaches the main drainage.

143

144   **2.2 Lahar Monitoring at Volcán de Colima**

145   In 2007, a monitoring program was implemented at Volcán de Colima. At the beginning,

146   two rain gauges where installed to study lahar initiation (AR and PH sites, Figure 1) and

147   lahar propagation was detected by the broadband seismic stations of RESCO, the

148   seismological network of Colima University (Davila et al., 2007; Zobin et al., 2009; Capra

149   et al., 2010). Afterwards, two monitoring station specifically designed for studying lahar

150   activity were installed, in 2011 at the Montegrande ravine and in 2014 at La Lumbre ravine

151   (MSMg and MSL respectively, Figure 1). Both stations consist of a 12 m-high tower with a

152   directional antenna transmitting data in real time to RESCO facilities, a camcorder

153   recording images each 2-4 secs with a 704 x 480 pixels in resolution, a rain gauge coupled

154   with a soil moisture sensor, and a 10 Hz geophone (Vázquez et al., 2016a; Coviello et al.,

155   under revision). The rain gauge (HOBO RG3) records rain accumulation at one-minute

156   intervals. At Montegrande ravine seismic data are also obtained from a 3 component Guralp

Natural Hazards
and Earth System
Sciences
Discussions

Open Access

EGU

157   CMG-6TD broadband seismometer installed at 500 m upstream from the monitoring site,

158   sampling at 100 Hz (BB-RESCO, Figure 1).

159   Montegrande station detected lahars occurred during 2011 Jova and 2013 Manuel events,

160   and lahars triggered during the 2015 Hurrican Patricia were only recorded by La Lumbre

161   station (Table 1). In fact, in 2011 only MgMS site was operating (as the BB-RESCO

162   station), and recorded the seismic signal of the lahar associated to Jova and Manuel. No

163   images are available since both events occurred during the night. The LMS station starts to

164   operate at the end of 2013 and was able to record the lahars associated to Hurricane Patricia

165   along the La Lumbre ravine (images and geophone data). In contrast, in 2015 the MgMS

166   was destroyed by pyroclastic flows during the 10-11 explosive activity, and in October

167   2015 the new station was still under construction. Only few pictures were acquired and they

168   are of low quality because of the abundant steam coming from the hot lahars since they

169   originated from the remobilization of fresh pyroclastic flow deposits (Capra et al., 2016).

170   The 11 June 2013 event was perfectly captured by the camera installed at the MgMS site

171   and the BB-RESCO recorded its seismic signal.

172   The seismic signal is here analyzed to detect the arrival of main flow fronts and discharge

173   variation. For this, only the amplitude of the signal is considered, which can be correlated

174   with the variation in the maximum peak flow discharge (Doyle et al., 2010; Vázquez et al.,

175   2016a). The seismic record is here compared with the available images to identify the main

176   changes in dynamic of the detected lahars. All the lahars here analyzed correspond to multi-

177   pulses events as classified by Vazquez et al. (2016a); they consist of long lasting lahars

178   presenting several pulses each one characterized by a block-rich front followed by the main

179   body and dilute tail showing continuous changes in flow discharges. A detailed seismic

180   description of these types of lahars is available in Vázquez et al. (2016a), here we focus on

181   the number of main flow peaks and their arrival times (Table 2).

182

183   **2.3. The hydrometeorological events**

184   Hurricane Jova formed over the Pacific Ocean, hit the Pacific coast on October 12, 2011, as

185   a category 2, and traveled inland toward Volcán de Colima. The hurricane arrived as a

186   tropical storm at the town of Coquimatlán, just 10 km SW of the city of Colima with winds

187   up to 140 km/h, and 240 mm of rain over 24 h (Fig. 3a). Severe damage was registered in

188   inhabited area, including the city of Colima where floods damaged roads, bridges and

189   buildings.

190   The 2013 Hurricane Manuel of category 1, hit the pacific coast during national holidays

191   (Fiestas Patria) causing several damage to mountainous region in Guerrero state, triggering

192   several landslides that caused up to 96 deaths and left several villages uncommunicated as

193   thousands of tourists trapped at Acapulco and Ixtapa international airports. At Volcan the

194   Colima rains started on September 15 and lasted for more than 30 hrs with more than 300

195   mm of accumulated rains (Fig. 3a).

196   The 2015 Hurricane Patricia was considered as the strongest hurricane on record to affect

197   Mexico. The system starts to develop on 18 October over the Pacific Ocean, strengthened

198   into a hurricane shortly after 00:00 GMT 22 October and early on 23 October it reached its

199   maximum category of 5. But late on the same day, the system rapidly lost its strength. It

200   landfalls around 23:00 GMT along the coast of the Mexican state of Jalisco near Playa

201   Cuixmala, about 60 km west-northwest of Manzanillo. On the morning of the 23 October,

Natural Hazards
and Earth System
Sciences
Discussions

202   2015 it continued to rapidly weaken as it moves on the Sierra Madre Occidental high

203   relieves. At Colima town, up to 400 mm of rains accumulated along 30 hours since the

204   morning of 23 October (Fig. 3a). Lahars along the Montegrande ravine were hot since they

205   originated from the erosion of pyroclastic flow deposits emplaced during the 10-11 July

206   2015 eruption. Sever damages affected the Colima town and the volcano surrounding. A

207   bridge along the interstate was destroyed leaving uncommunicated La Becerrara village and

208   interrupting the traffic between Colima and Jalisco states.

209   Patricia and Manuel rainfalls show a similar behavior, with a progressive rain accumulation

210   along 28-30 hrs; in contrast, during Hurricane Jova, 200 mm of rain accumulated in less

211   than 15 hrs reaching a total of 240 mm during the following 13 hrs (Fig. 3a). These

212   differences are more evident plotting the 10-min accumulated value normalized over the

213   total accumulated rainfall (Fig. 3b). Average rainfall intensities calculated over a 10-min

214   interval range from 32 mm/hrs to 37 mm/hrs for Manuel and Patricia events respectively

215   and up to 43 mm /hrs for the Hurricane Jova (Table 2). Finally rainfall values were

216   calculated at selected intervals (15 m, 30 m, 45 mm, 1, 3, 6, 12, 18, 24, 28 hr) to design

217   possible storm rainfall distributions based on tropical rains associated to hurricanes

218   recorded so far at Colima Volcano (Table 2). Considering the similar behavior of the

219   Manuel and Patricia rainfalls, a stormwater can be designed considering their average

220   values (Fig. 3c) (i.e. NRCS, 2008), based on which a forecast analysis can be performed, as

221   will be discussed below.

222

223   **2.4. Rainfall simulations**

Natural Hazards
and Earth System
Sciences

Discussions

224   To better understand the lahar behavior and duration during extreme hydrometeorological

225   event at Volcán de Colima, rainfall simulations were performed with Flo-2D code (O´Brian

226   et al., 1993). The Flo-2D code routes the overland flow as discretized shallow sheet flow

227   using the Green-Ampt or the SCS Curve number (or combined) infiltration models. For the

228   present work the SCS Curve Number (SCS-CN, i.e. Mishra and Singh, 2003) was selected.

229   With this model, the volume of water runoff produced for the simulated precipitation is

230   estimated through a single parameter that summarizes the influence of both the superficial

231   aspects and deep soil, including the saturated hydraulic conductivity, type of land use, and

232   humidity before the precipitation event. A similar approach was already used for modeling

233   debris flow initiation mechanisms (i.e. Gentile et al., 2006; Llanes et al., 2015). To apply

234   the SCS-CN model, it is necessary to classify the soil in one of four groups, each

235   identifying a different potential runoff generation (A, B, C, D; USDA-NRCS 2007). The

236   watershed of La Lumbre and Montegrande ravines were subdivided in two main zone; the

237   unvegetated upper cone and the main channel that consist of unconsolidated pyroclastic

238   material with large boulders imbedded in sandy to silty matrix, and the vegetated lateral

239   terraces. Lateral terraces consist of old pyroclastic sequences, with incipient soils and

240   vegetated with pine trees and sparse brushes, with soils that show a hydrophobic behavior

241   at the beginning of the rain season (Capra et al., 2010). In-situ infiltration tests were also

242   performed based on which values of saturated conductivity were obtained in the range of 50

243   mm/h (nude soil) to 100 mm/h (vegetated) (Ortiz, 2017). Based on these observations, soils

244   were classified between group A and B (Bartolini and Borselli, 2009). Curve Numbers for

245   the vegetated terraces and for the nude soils were estimated in 75 and 80 respectively (in

246   wet season, Hawkins et al., 1985; Ferrer-Julia et al. 2003). To perform simulation with the

247   FLO-2D code, two polygons were traced to delimit the un-vegetated portion of the cone

248   from the vegetated area of the watershed, and at each polygon the relative CN value was

249   assigned. The simulated rain corresponds with the cumulative value calculated at 10

250   minutes interval (Fig. 3b). At the apex of each watershed a barrier of outflow points were

251   defined to obtain the total values of the watershed discharge. The simulation was performed

252   with a 20-m digital elevation model.

253

3. Results

255   During the Jova hurricane, lahars started in Montegrande ravine early in the morning of 12

256   October, 2011, around 07:20 GMT (here after all time is in GMT), after approximately 40

257   % of the total rain (240 mm) accumulated (Fig. 4a). The event lasted more than 4 hours,

258   and three main peaks in amplitude can be detected in the seismic signal (Fig. 4a). In

259   particular, the first two peaks are similar in amplitude (0.015 cm/s), separated by more than

260   2 hours of signal fluctuation. After less than one hour from the second peak, a single,

261   discrete pulse can be recognized (0.05 cm/s in amplitude), followed by a "train" of low-

262   amplitude seismic peaks that lasted for more than an hour.

263   Along the same ravine, an extreme event was recorded on 11 June, 2013. This event

264   corresponds to an extraordinary episode and is here introduced to better discuss the

265   hydrological response of the Montegrande ravine. It represents an unusual event at the

266   beginning of the rainy season, considering the total accumulated rainfall of 120 mm in less

267   than 3 hrs (Table 2), with maximum pick intensity up to 140 mm/hr (Fig. 4b). Based on the

268   seismic record and the still images of the event, this lahar was previously characterized as a

269   multi-pulse flow, with three main blocks-rich fronts (I, II and IV, Fig. 4c), with similar

Natural Hazards
and Earth System
Sciences
Discussions

Open Access

EGU

270   amplitudes (0.015-0.025 cm/s), followed by a main flow body consisting of a homogenous

271   mixture of water and sediments (with a sediment concentration at the transition between a

272   debris flow and an hyperconcentrated flow) (III, Fig. 4c) (Vazquez et al. 2016a). The last,

273   more energetic pulse (0.042 cm/s) was accompanied by a water-rich frontal surge that was

274   able to reach the lens of the camera (IV, Fig. 4c). Comparing the Jova and the 2013 event

275   seismic records it is possible to note that in both events, the largest pulse corresponds with

276   the last one. Flow discharge was estimated for the 2013 event, with a maximum of 120 m^3/s

277   value for the largest pulses (IV, Figure 4b) (Vazquez et al., 2016a). For the Jova event, the

278   only visual data available are the images of the channel the day before and the day after the

279   event, where a deep erosion of the channel is visible (Fig. 5), but comparing its seismic

280   signal with the 2013 lahar, and based on the classification criterion established for lahars at

281   Volcán de Colima (Vazquez et al., 2016a) each main peak corresponds to the arrival of

282   flow surges or to block-rich fronts followed by the body of the flow. Fluctuation in seismic

283   energy along the vertical component reflects variation in flow discharge.

284   The lahar recorded during the Hurricane Manuel along the Montegrande ravine shows a

285   similar behavior as described for the Jova event (Fig. 6). As the event occurred during the

286   night no images are available. Based on the seismic record from the BB-RESCO, lahars

287   stated around 03:00, and lasted for seven hours. The event was characterized by five main

288   pulses, which amplitude increases with time (0.012-0.025 cm/s), being the last one the

289   larger in magnitude (0.04 cm/s). Based on the amplitude values, the first two peaks

290   correspond to precursory dilute flow waves followed by the three main pulses with block-

291   rich fronts (I, II and III, Fig 6).

Natural Hazards
and Earth System
Sciences
Discussions

292   For the Hurricane Patricia seismic data (from the geophone) and still images were recorded

293   at the La Lumbre monitoring station. Based on these data, at approximately 21:22 a slurry

294   flow is detected on the main channel (Fig. 7a). First pulses of hyperconcentrated flows were

295   detected around 01:30 (24 October) which progressively increased in flow discharge and

296   sediment concentration. Several front waves were observed during flooding (I and II, Fig.

297   7b) for which an average flow discharge of 80-100 m^3/sec was estimated, and two main

298   pulses arrived at 04:30 and 05:00, with 6 m-depth block-rich fronts and maximum flow

299   discharge of 900 m^3/sec (III, IV, V and VI, Fig. 7b). At around 05:40 the seismic record

300   detected the arrival of a third pulse. Although no images were available, the amplitude of

301   the last pulse (0.07 cm/s) suggests it was larger than those previously described. As

302   observed for the three events recorded at Montegrande ravine, the largest pulse correspond

303   again with the last one.

304   The results of rainfall simulations are plotted as a normalized curve of the total discharge,

305   along with the normalized accumulated rainfall and its intensity (calculated over a 10-min

306   interval) (Fig. 8). In the same plot, the arrival time of the main lahar pulses here analyzed is

307   also indicated (red triangles, Fig. 8). By comparing watershed discharge with rainfall

308   intensity, a general correlation can be observed for the Montegrande basin during Jova and

309   Manuel hurricane, contrasting with the June 2013 event, where the simulation is not able to

310   reproduce watershed discharge during the first minutes of the event when most of rainfall is

311   accumulated and maximum rainfall intensities are detected. For la Lumbre watershed a

312   clear correlation between peak intensities and watershed discharge is not clearly

313   observable. If the arrival times of the main lahars' pulses are considered, the events

314   associated to the hurricanes Jova and Manuel along the Montegrande ravine show a similar

14

315 behavior. In both cases early slurry flows are detected after ~40% of the total rain is

316 accumulated. The main flow pulses better correlate with the highest rain intensity values,

317 which also correspond with maximum peaks in watershed discharge; the last, largest pulse

318 corresponds with the maximum peak discharge of the watershed. In contrast, for the

319 Patricia event, along the La Lumbre ravine, first slurry flows also starts after 40% or

320 rainfall accumulated, but main lahar pulses fit better with the peaks watershed discharge.

321 Finally, analyzing the simulation in the Montegrande ravine for the June 2013 event, it is

322 possible to observe a different behavior. The lahar starts as less than the 10% of rain is

323 accumulated, and the main lahar pulses perfectly correlate with the peak rainfall intensities,

324 and only the last largest pulse correlates with the watershed peak discharge.

325

326 **4. Discussion**

327 At present, several attempts to define lahar rainfall thresholds have been already carried out

328 for different volcanoes (i.e. Lavigne et al., 2000; van Westen and Daag, 2005 Barclay et al.,

329 2007), including Volcán de Colima (Capra et al., 2010). This study is mostly addressed to

330 better predict the lahar evolution during extraordinary hydrometeorological event as

331 hurricane, a common long-duration and large-scale rainfall phenomenon at tropical

332 latitudes. In particular, we are interested in predicting the arrival of block-rich fronts that

333 have caused several damages during past events. Based on the seismic and visual data

334 gathered from the events here analyzed, it is possible to evidence which are the key factors

335 in controlling the arrival of main lahars fronts. For Jova, Manuel and Patricia events, lahars

336 started after the 40% of total rain accumulated, and apparently the timing for the initial

337   pulses correlate well with the peaks of the rainfall intensity for the Montegrande ravine,

338   while for la Lumbre ravine they better match with the watershed discharge. Nevertheless

339   for all analyzed cases, the largest pulses correspond with the last ones and correlate with the

340   peak watershed discharge for all the analyzed examples. The observed difference between

341   Montegrande and La Lumbre ravines can be correlated with the different areas and shapes

342   of the two catchments. In fact, due to its elongated shape (K_G = 1.7) and small area (A = 2

343   km), the Montegrande watershed shows a quicker response between rainfall and discharge,

344   with a rapid water runoff that concentrated at different point along the main channel (Fig.

345   1b). This behavior is much clearer for the June 2013 event, which occurred at the beginning

346   of the rain season when soils on the lateral terraces of the ravines show a hydrophobic

347   behavior (Capra et al., 2010). The simulation is not able to reproduce any watershed

348   discharge at the beginning of the event, because the hydrophobic behavior of the soils

349   inhibits the infiltration and the water runoff quickly promotes lahar initiation. During this

350   event, the first lahar pulses perfectly match with the rainfall peak intensities (except for the

351   last major pulse), starting from the very beginning of the rainfall event. In contrast, La

352   Lumbre ravine has a wider, rounded upper watershed (K_G = 1.1; A = 14 km^2) that is able to

353   concentrated a larger volume of water before to turn SW in the main channel where lateral

354   contribution can still increase water discharge. Even if rainfalls of hurricanes Manuel and

355   Patricia show a similar behavior (Fig. 3), the catchment response of La Lumbre is clearly

356   different with a pulsating behavior of lahars mainly controlled by the watershed discharge.

357   Nevertheless, for all the events here analyzed, the largest pulse corresponds with the last

358   one recorded and it correlates with the maximum watershed discharge, pointing to a strong

359   control of the catchments recharge in generating the largest and more destructive pulses.

360   Previous works correlated the occurrence of surges within a lahar to multiple sources, such

Natural Hazards
and Earth System
Sciences
Discussions

EGU
Open Access

361 as lateral tributaries along the main channel (i.e. Doyle et al., 2010) or due to the failure of

362 temporary dams of large clasts in correspondence of an increase in rainfall intensity (Kean

363 et al., 2013). Lateral tributaries are absent in both Montegrande and La Lumbre channels

364 and, even if accumulation of clasts it is possible, no significant discontinuities of the

365 channel bed can be observed upstream the monitoring sites. Based on data here presented,

366 formation of pulses within a lahar is mostly controlled with the increase in water runoff that

367 at a critical discharge rate mobilize a large volume of sediment where large clasts

368 accumulate at its front. This is a well-documented mechanism (i.e. Iverson, 1997), but

369 based on the model here proposed, the discharge rate is controlled by the watershed

370 discharge that regulates the timing on the arrival of main pulses, depending on the rainfall

371 behavior and the watershed shape. Nevertheless, the last pulse always is the largest in

372 volume. This model is strictly related to migratory, long-duration and large-scale rainfall

373 events hitting tropical volcanoes such as the Volcán de Colima. In fact, during mesoscale

374 non-stationary rainfalls, typical at the beginning of the rainy season, lahars are usually

375 triggered at low accumulated rainfall values and controlled by rainfall intensity due to the

376 hydrophobic behavior of soils, and they usually consist of uni-pulse events with a single

377 block-rich front that last less than one hour (i.e. Vázquez et al., 2016b). In perspective, the

378 results here presented can be used to design an Early Warning System (EWS) for hurricane-

379 induced lahars, i.e. event triggered by long-duration and large-scale rainfalls. Most

380 common pre-event or advance-EWSs for debris flows are based on empirical correlations

381 between rainfall and debris flow occurrence (e.g., Keefer et al., 1987; Aleotti, 2004; Baum

382 and Godt, 2009). The instruments adopted for debris-flow advance warning are those

383 normally used for hydrometeorological monitoring and consist of telemetry networks of

384 rain gauges and/or weather radar. The typical way to represent these relations is identifying

385   critical rainfall thresholds for debris flow occurrence. The availability of both a large

386   catalogue of events and a reliable precipitation forecast that could give the predicted

387   amount of rainfall some hours in advance would allow the issue of an effective warning, at

388   least in predicting the arrival time of the main lahar pulses. In addition, instrumental

389   monitoring of in-channel processes can be used to validate a preliminary warning-condition

390   triggered by wheatear forecast and/or rainfall measurements.

391

392   **5. Conclusions**

393   Real time monitoring of lahars at Volcán de Colima volcanoes reveal that watershed

394   discharge is the key factor in controlling the arrival of main block-rich fronts during long-

395   lasting lahar triggered during tropical storms, and that the largest destructive pulses will

396   arrive after the initial surging. For the 2015 Hurricane Patricia event the weather forecast

397   predicted an estimated value for the total rainfall, as also the approximate time of its

398   landfall. Based on the deigned storm obtained with the time rainfall distribution of the

399   event here analyzed, it could have been possible to anticipate when lahars started along the

400   La Lumbre ravine, and the arrival time of main pulses. Along the other ravines, that show a

401   watershed similar to the Montegrande, it could have been possible to predict the arrival of

402   at least the largest pulse. This information coupled with the real time monitoring could be a

403   better tool for hazard assessment and risk mitigation. In fact, these findings can be used to

404   implement an advance warning system based on the monitoring of a hydrometeorological

405   process to issue a warning before a possible lahar is triggered.

406

Natural Hazards
and Earth System
Sciences

Open Access

EGU

Discussions

413

414   **References**

415   Aleotti P (2004) A warning system for rainfall-induced shallow failures. Eng. Geol. 73(3-

416   4): 247–265.

417   Barclay J, Alexander J, Susnik L (2007) Rainfall-induced lahars in the Belham valley,

418   Monserrat, West Indies. Journal of the Geological Society of London 164: 815-827.

419   Bartolini D, Borselli L (2009) Evaluation of the HydrologicSoil Group (HSG) with the

420   Procedure SCS Curve Number. In: Manualof Methods for Soil and Land Evaluation,

421   Edoardo A, Costantini C (ed), Science Publisher Inc., 600 pages. ISBN 978-1-57808-571-2

422   Baum R L, Godt JW (2009) Early warning of rainfall-induced shallow landslides and debris

423   flows in the USA. Landslides 7(3): 259–272.

424   Bendjoudi H, Hubert P (2002) Le coefficient de Gravélius : analyse critique d'un indice de

425   forme des bassins versants. J. Sci. Hydrol. 47: 921–930.

426   Capra L, Borselli L, Varley N, Norini G, Gavilanes-Ruiz JC Sarocchi D, Caballero L

427   (2010) Rainfall-triggered lahars at Volcán de Colima, Mexico: surface hydro-repellency as

428   initiation process. Journal of Volcanology and Geothermal Research 189(1-2): 105-117.

429   Cortes A, Macias JL, Capra L, Garduño-Monroy VH (2010) Sector collapse of the SW

430   flank of Volcán de Colima, México. The 3600 yr BP La Lumbre-Los Ganchos debris

431   avalanche and associated debris flows. Journal of Volcanology and Geothermal Research

432   197: 52-66.

433   Coviello V, Capra L, Vázquez R, Marquez-Ramirez V, under revision. Seismic

434   characterization of hyperconcentrated flows in volcanic environment. Earth Surface

435   Processes and Landforms.

436   Cronin SJ, Hodgson KA, Neall VE, Palmer AS, Lecointre JA (1997) 1995 Ruapehu lahars

437   in relation to the late Holocene lahars of Whangaehu River, New Zealand. New Zealand

438   Journal of Geology and Geophisics 40: 507-520.

439   Davila N, Capra L, Gavilanes JC, Varley N, Norini G (2007) Recent lahars at Volcán de

440   Colima (Mexico): drainage variation and spectral classification. Journal of Volcanology

441   and Geothermal Research 165: 127-141.

442   de Bélizal E, Lavigne F, Hadmoko DS, Degai JP, Dipayana GA, Mutagin BW, Marfai MA,

443   Coquet M, Le Mauff B, Robin AK, Vidal C, Cholik N, Aisyah N (2013) Rain-triggered

444   lahars following the 2010 eruption of Merapi volcano, Indonesia: A major risk. Journal of

445   Volcanology and Geothermal Research 261: 330-347.

446   Doyle EE, Cronin SJ, Cole SE, Thouret JC (2010) The coalescence and organization of

447   lahars at Semeru volcano, Indonesia. Bulletin of Volcanology 72(8): 961-970.

448   Dumaisnil C, Thouret JC, Chambon G, Doyle EE, Cronin SJ (2010) Hydraulic, physical

449   and rheological characteristics of rain-triggered lahars at Semeru volcano, Indonesia. Earth

450   and Surface Processes and Landform 35: 1573-1590.

451   Ferrer-Julio M, Estrela T, Sanchez del Corral Jimenez A, Garcia-Melendez E (2003)

452   Generation of a curve number map with continuous values based on saturated hydraulic

453   conductivity. XI World Water Congress, 5-9 October 2003, Madrid, Spain: 1-10.

454   http://iwra.org/member/index.php?mainpage=&page=286&congressyear=2003

455   Gentile F, Bisantino T, Puglisi S, Trisorio Liuzzi G (2006) Analysis and modeling of debris

456   flows in Gargano watersheds (Puglia region, Southern Italy). WIT Transactions on Ecology

457   and the Environment 90: 181-191.

458   Hawkins RH, Hjelmfelt AT, Zevenbergen AW (1985) Runoff probability storm depth and

459   curve numbers. Journal of the Irrigation and Drainage Division 111: 330-340.

460   Kean W, McCoy S, Tucker G, Staley D, Coe J (2013) Runoff-generated debris flows:

461   Observations and modeling of surge initiation, magnitude, and frequency. Journal of

462   Geophysical Research: Earth Surface 118: 1-18.

463   Keefer DK, Wilson RC, Mark RK, Brabb EE, Brown WM, Ellen SD, Harp EL, Wieczorek,

464   GF, Alger CS, Zatkin RS (1987) Real-time landslide warning during heavy rainfall.

465   Science 238(4829): 921–5.

466   Iverson RM (1997) The physics of debris flows: Reviews of Geophysics 35: 245-296.

Natural Hazards
and Earth System
Sciences
Discussions

467 Lavigne F, Thouret JC, Voight B, Suwa H, Sumaryono A (2000) Lahars at Merapi volcano,

468 Central Java: an overview. Journal of Volcanology and Geothermal Research 100: 423-456.

469 Lavigne F, Thouret JC (2002) Sediment transport and deposition by rain-triggered lahars at

470 Merapi Volcano, Central Java, Indonesia. Geomophology 49: 45-69.

471 Llanes F, Ferrer PK, Gacusan R, Realino V, Obrique J, Eco RN, Lagmay AMF (2015)

472 Scenario-based maps using flo-2d and IFSAR-derived digital elevation models on the

473 November 2006 rainfall-induced lahars, Mayon Volcano, Philippines. ACRS 2015

474 Proceedings, Asian Association on Remote Sensing.

475 Marchi L, Arattano M, Deganutti A. (2002) Ten years of debris-flow monitoring in the

476 Moscardaro Torrent (Italian Alps), Geomorphology 46: 1–17, doi:10.1016/S0169-

477 555X(01)00162-3.

478 Mishra S K, Singh VP (2003) Soil conservation service curve number (SCS-CN)

479 methodology. Kluwer Academic Publishers, Dordrecht, Netherlands.

480 Natural Resource Conservation Services (2008) Rainfall-Frequency and Design Rainfall

481 Distribution for Selected Pacific Islands. Engineering Technical Note No. 3, United States

482 Department of Agriculture:115 pp.

483 O'Brien J, Julien P, Fullerton W (1993) Two-dimensional water flood and mudflow

484 simulation. J. Hydraul. Eng.-ASCE 119: 244-261.

485 Ortiz A. (2017) Modelado de conectividad y contribución de escorrentía superficial lateral

486 en la dinámica de flujos granulares de áreas volcánicas activas. PhD thesis, Universidad

487 Autónoma de San Luis Potosí, Facultad de Ciencias, México: 224 pp.

488   Ortiz-Rodríguez AJ, Borselli L, Sarocchi D (2017) Flow connectivity in active volcanic

489   áreas: use of index of connectivity in the assessment of lateral flow contribution to main

490   streams. Catena 157: 90 – 111.

491   Roverato M, Capra L, Sulpizio R, Norini G (2011) Stratigraphic reconstruction of two

492   debris avalanche deposits at Colima Volcano (Mexico): Insights into pre-failure conditions

493   and climate influence. Journal of Volcanology and Geothermal Research 207: 33-46.

494   Scott KM, Vallance JV, Kerle N, Macias JL, Strauch W, Devoli G (2005) Catastrophic

495   precipitation-triggered lahars at Casita Volcano, Nicaragua: occurrence, bulking and

496   transformation. Earth Surface Processes and Landforms 30: 59-79.

497   Sheridan MF, Connor CB, Connor L, Stinton AJ, Galacia O, Barrios G (2007) October

498   2005 Debris Flows at Panabaj, Guatemala: Hazard Assessment. American Geophysical

499   Union, Spring Meeting 2007, abstract #V33A-07.

500   Takahashi T (2007) Debris Flow: Mechanics Prediction, and Countermeasures. Taylor and

501   Francis/Balkema, Leiden: 448 pp.

502   Umbal JV, Rodolfo KS (1996) The 1991 lahars of southwestern Mount Pinatubo and

503   evolution of the lahar-dammed Mapanuepe lake. Fire and mud; eruptions and lahars of

504   Mount Pinatubo, Philippines, P. I. o. V. a. Seismology, ed., Quezon, Philippines: pp. 951-

505   970.

506   USDA-NRCS (U.S. Department of Agriculture-Natural Resources Conservation Service).

507   (2007) Hydrologic soil groups. National engineering handbook. Part 630 hydrology,

508   Washington, DC.

509   van Westen CJ, Daag AS (2005) Analysing the relation between rainfall characteristics and

510   lahar activity at Mount Pinatubo, Philippines. Earth and Surface Processes and Landform

511   30: 1663-1674.

512   Van Wyk Vries B, Kerle N, Petley D (2000) Sector collapse forming at Casita volcano,

513   Nicaragua. Geology 28(2): 167-170.

514   Vázquez R, Suriñach E, Capra L, Arámbula-Mendoza R, Reyes-Dávila G (2016a) Seismic

515   characterisation of lahars at Volcán de Colima, Mexico. Bulletin of Volcanology 78: 8.

516   Vázquez R, Capra L, Coviello V (2016b) Factors controlling erosion/deposition

517   phenomena related to lahars at Volcán de Colima, Mexico. Natural Hazards and Earth

518   System Sciences 16: 1881–1895.

519   Zanuttigh B, Lamberti A (2007) Instability and surge development in debris flows. Rev.

520   Geophys. 45: RG3006, doi:10.1029/2005RG000175.

521   Zobin VM, Placencia I, Reyes G, Navarro C (2009) The characteristics of seismic signal

522   produced by lahars and pyroclastic flows: Volcán de Colima, Mexico. Journal of

523   Volcanology and Geothermal Research 179: 157-167.

524

Natural Hazards
and Earth System
Sciences
Discussions

Figure captions

Figure 1. a) Aster image (4, 5 and 7 bands in RGB combination) where main watersheds at Volcán de Colima are represented. The locations of the monitoring stations are indicated. The inset show the location of the raingauge of the Meteorological National Service at the summit of the Nevado de Colima Volcano.

Figure 2. a) Panoramic view of the Volcán de Colima showing the unvegetated main cone mostly composed by loose volcanic fragments. b) Montegrande and c) La Lumbre ravines in the middle reach where it is possible to observe the main channel flanked by 10-15m-high terraces mainly constituted by debris avalanche deposits.

Figure 3. a) Cumulative and b) normalized values of rainfall of hurricanes Jova, Manuel and Patricia calculated at 10 min-intervals. c) Normalized curve of total rainfalls cumulated at 15, 30, 60 minutes and 1, 3, 6, 12, 18, 24, 28 hrs. Dotted line represents the average value between Manuel and Patricia hurricanes.

Figure 4. a) Seismic record of the lahar triggered during the Hurricane Jova, on 12 October, 2011. b) Seismic record of the lahar triggered during the 11 June, 2013 events. Main pulses are indicated with roman letters. c) Images captures by the camera corresponding to the main lahar pulses as indicated in figure b.

Figure 5. Images showing the morphology of the channel at the monitoring site of the Montegrande ravine, a) the day before and b) the day after the Hurricane Jova. c) Topographic profiles showing that the channel was eroded 1.5 m in depth.

545   Figure 6. Seismic record of the lahar triggered during the Hurricane Manuel, on 15

546   September, 2013, recorded along the Montegrande ravine

547   Figure 7. a) Seismic record of the lahar triggered during the Hurricane Patricia, on 26

548   October, 2015, recorded along the La Lumbre ravine. Main lahar pulses are indicated with

549   roman letters. b) Images captured by the camera corresponding to the main pulses as

550   indicated in figure a.

551   Figure 8. Diagrams showing the main lahar pulses (red triangles) as detected from the

552   seismic signal of the analyzed events in relation with the accumulated rainfall (dark line),

553   rainfall intensity (10m/hr) (gray line) and simulated watershed discharge (blue line) for the

554   following hidrometeorological events a) Jova; b) Manuel; c) 13 June, 2013; and d) Patricia.

555   Table 1. Data collected for the events here studied.
556

557   Table 2. Normalized accumulated rains (in percentage) at progressive time steps.

558

559   Table 1. Data collected for the events here studied.

Event	ravine	Seismic record	Image record	Total rain (mm)	Max. rain intensity (mm/hr)
Jova	Montegrande			240	43
Manuel	Montegrande	X		300	32
Patricia	Lumbre	X	X	400	37
11 June 2013	Montegrande	X	X	120	140

560

561

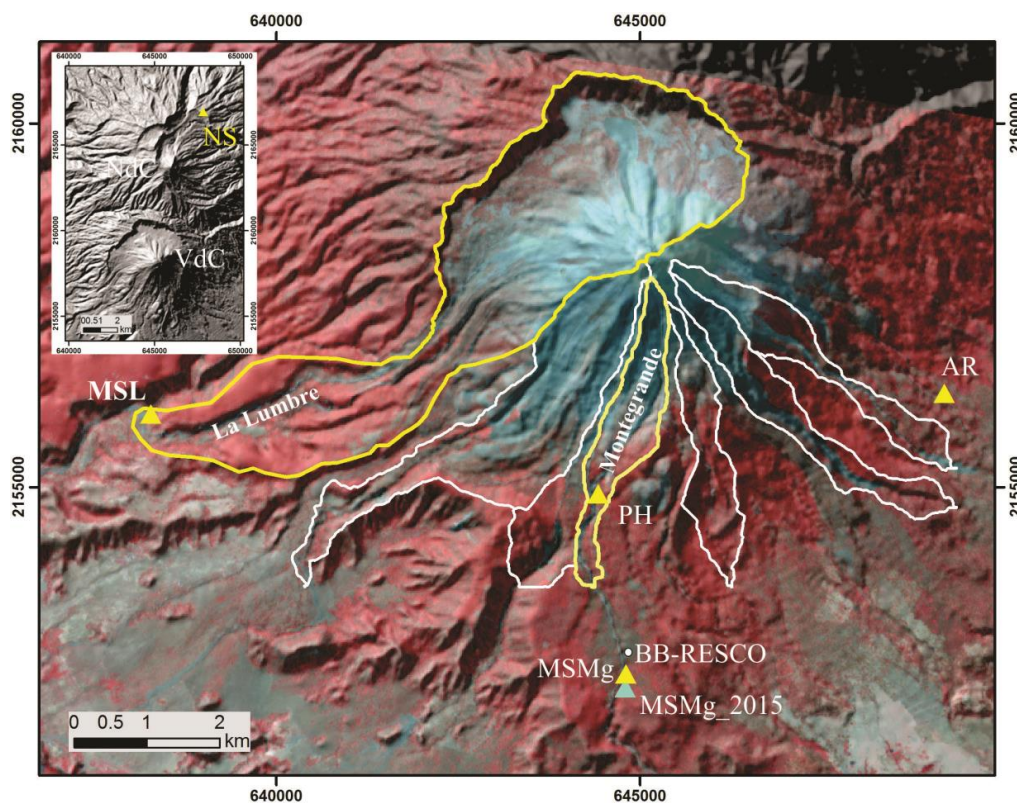562   Table 2. Normalized accumulated rains (in percentage) at progressive time steps.

Event/time (hrs)	0.25	0.5	1	2	3	6	12	24	27
Jova	0.0011	0.0016	0.0035	0.0172	0.0329	0.1411	0.7073	0.968	0.9943
Manuel	0.0023	0.0035	0.0042	0.0072	0.0151	0.0341	0.1548	0.735	0.9181
Patricia	0.0002	0.0004	0.0009	0.0062	0.0174	0.0556	0.2544	0.829	0.9782
average	*0.00125*	*0.00195*	*0.00255*	*0.0067*	*0.01625*	*0.04485*	*0.2046*	*0.782*	*0.9481*

563   The average values refer to hurricanes Manuel and Patricia.

564

565   Fig. 01

566

567

Natural Hazards
and Earth System
Sciences

Discussions

568   Fig. 02
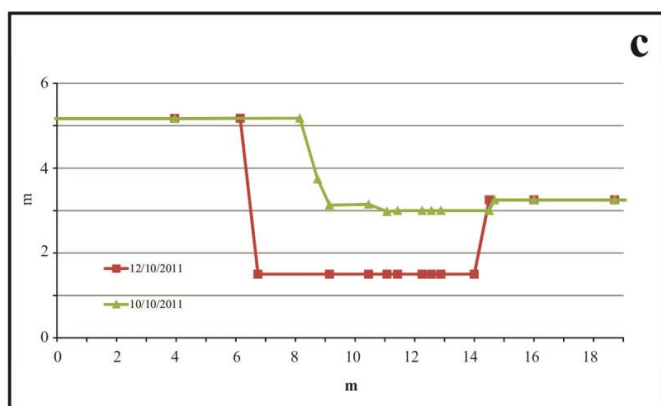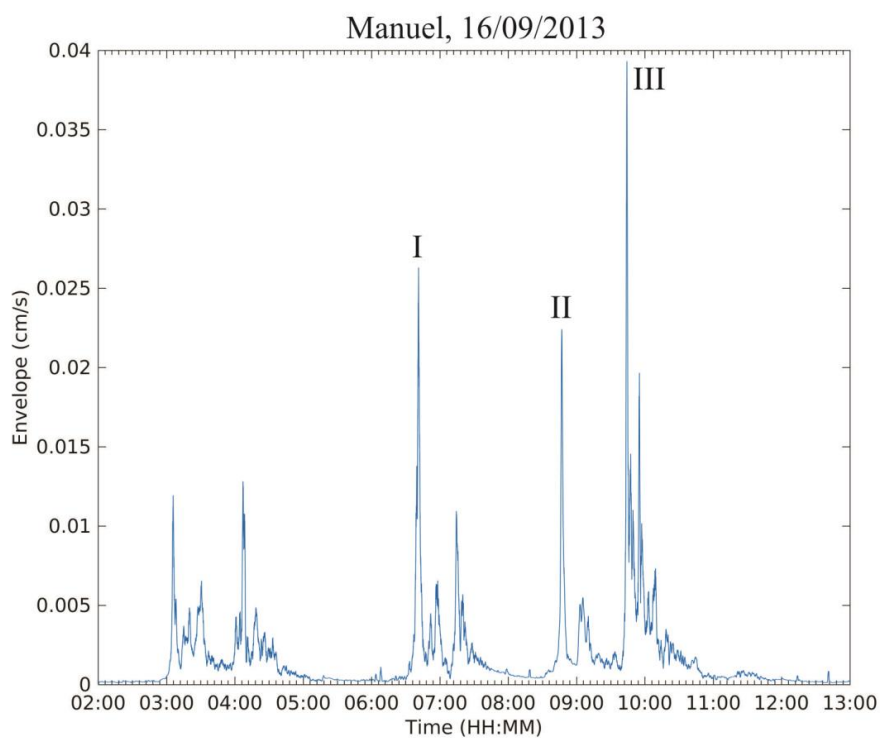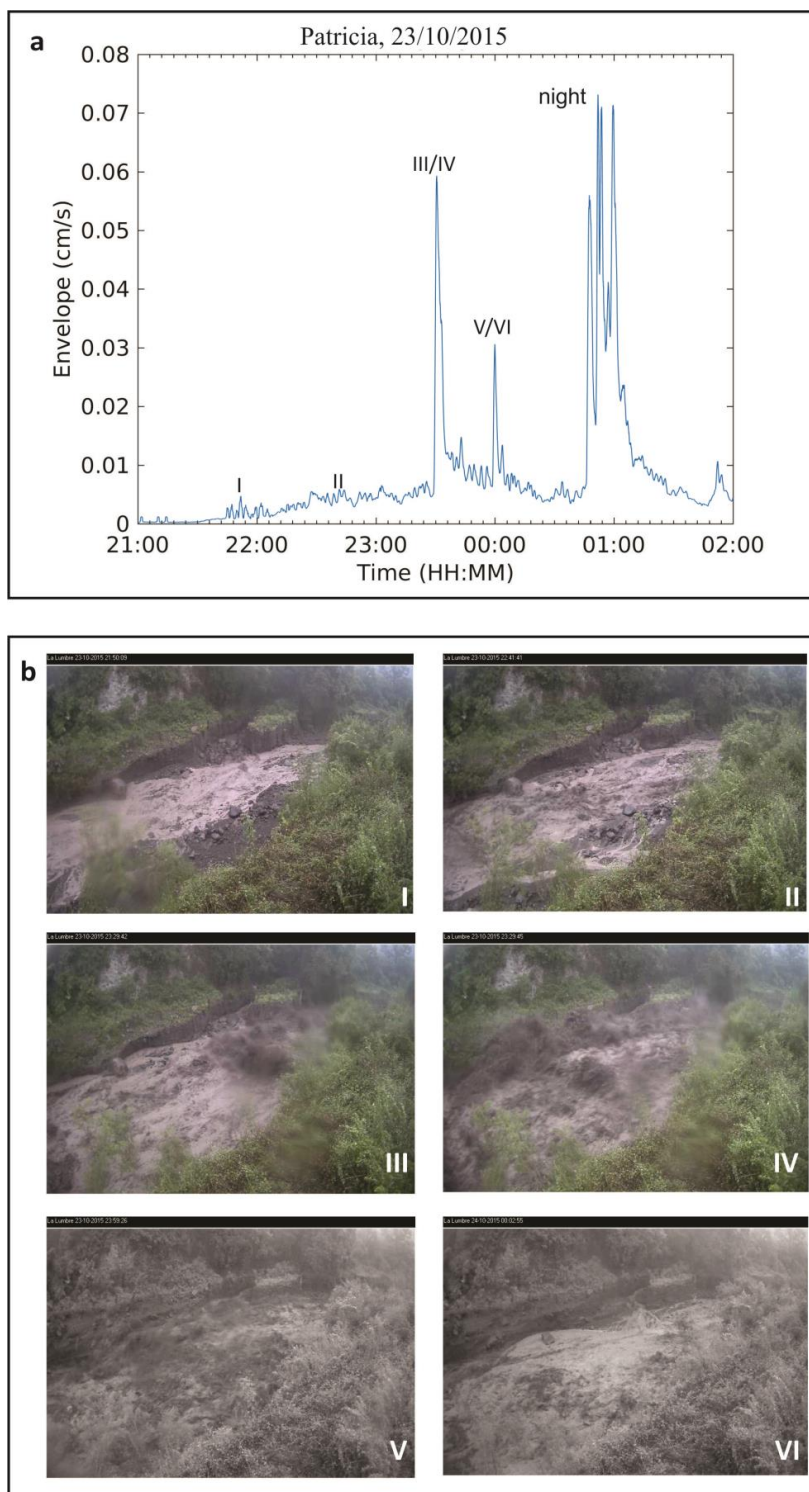

569

570

571   Fig- 03
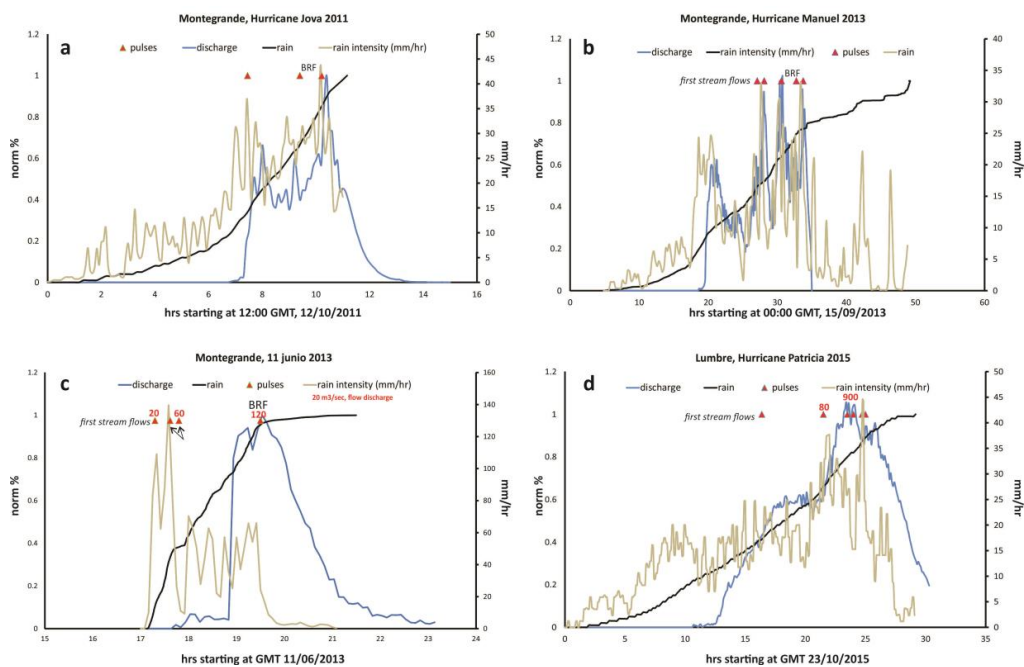
572
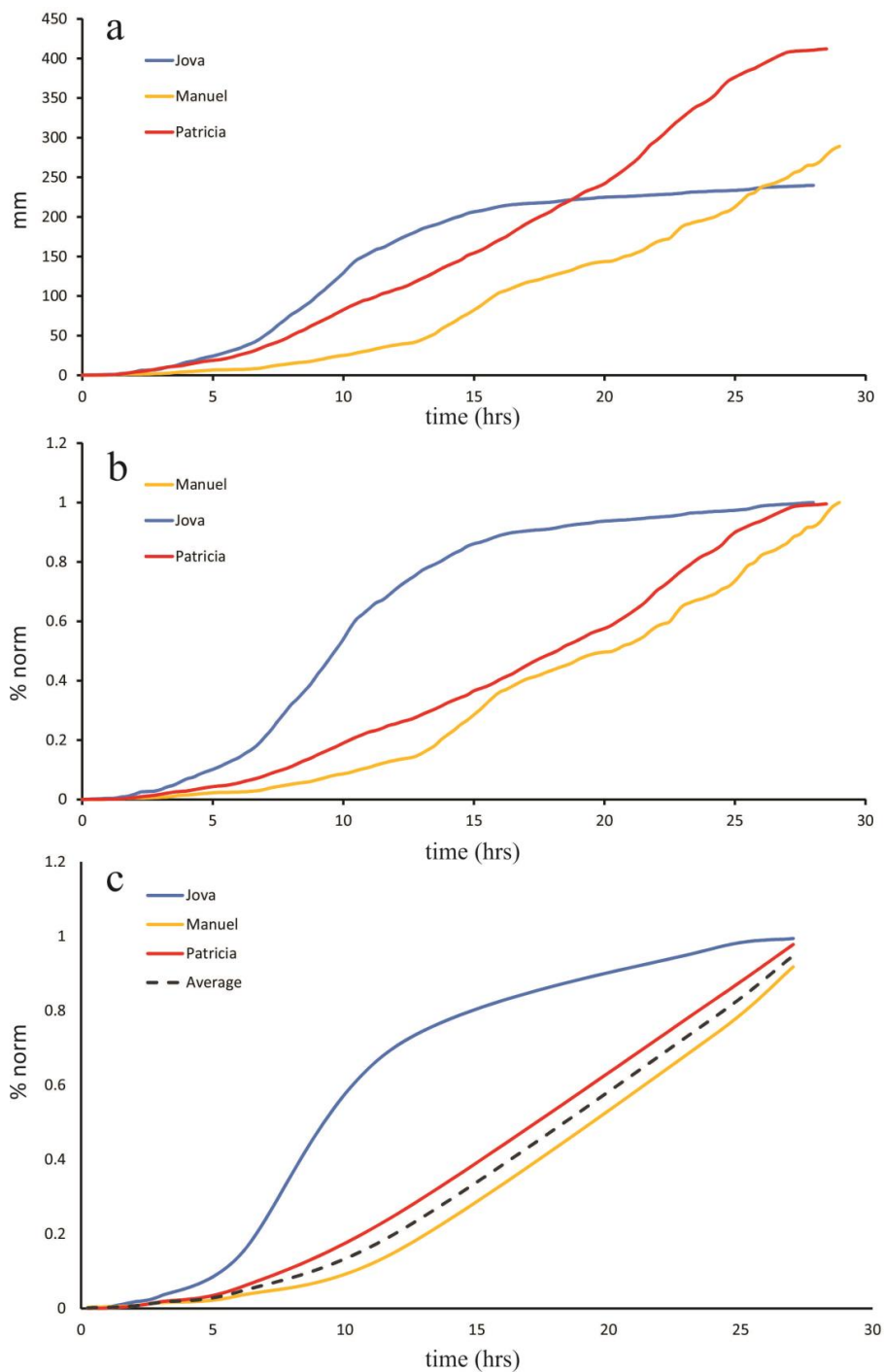
573   Fig. 04
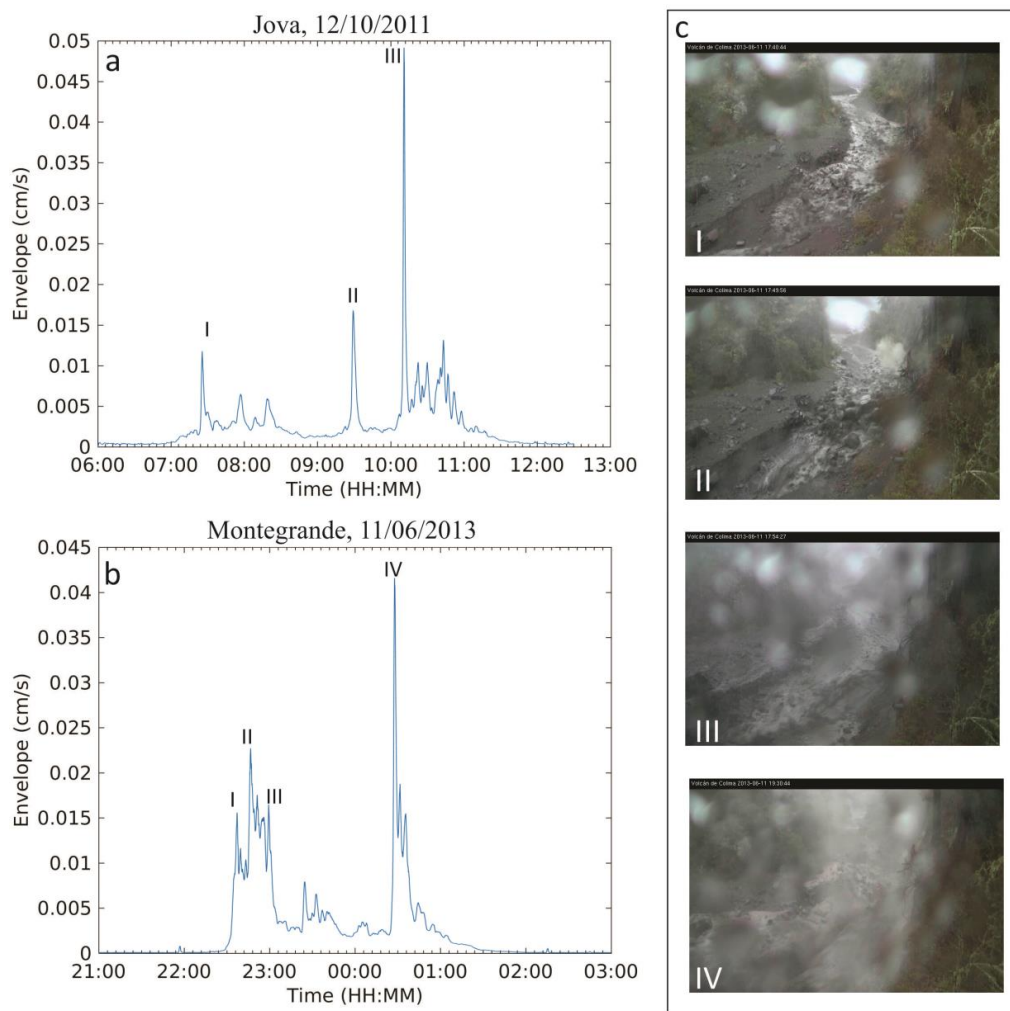
574

575

576   Fig. 05

577   Fig. 06

578

579   Fig. 07

35

Natural Hazards
and Earth System
Sciences
Discussions
Open Access
EGU

580   Fig. 08

581

582